
Article:
Ramesh, K, Smith, AK, Garcia, RR et al. (2020) Long-Term Variability and Tendencies in Middle Atmosphere Temperature and Zonal Wind From WACCM6 Simulations During 1850–2014. Journal of Geophysical Research: Atmospheres, 125 (24). ISSN: 2169-897X

https://doi.org/10.1029/2020jd033579

JGR Atmospheres

RESEARCH ARTICLE
10.1029/2020JD033579

Long-Term Variability and Tendencies in Middle Atmosphere Temperature and Zonal Wind From WACCM6 Simulations During 1850–2014

K. Ramesh[1,2], Anne K. Smith[1], Rolando R. Garcia[1], Daniel R. Marsh[1,3], S. Sridharan[4], and K. Kishore Kumar[5]

[1]Atmospheric Chemistry Observations and Modeling (ACOM) Laboratory, National Center for Atmospheric Research (NCAR), Boulder, CO, USA, [2]University Corporation for Atmospheric Research (UCAR), Boulder, CO, USA, [3]School of Physics and Astronomy, University of Leeds, Leeds, UK, [4]National Atmospheric Research Laboratory (NARL), Gadanki, India, [5]Space Physics Laboratory, Vikram Sarabhai Space Centre (VSSC), Trivandrum, India

Key Points:

- The variability of middle atmosphere temperature and zonal wind since the preindustrial period is derived from WACCM6 simulations
- Cooling associated with increasing CO_2 dominates the long-term trend at all levels in the middle atmosphere
- Multiple linear regression could not completely separate the cooling effects of CO_2 and ozone depleting substances

Correspondence to:
K. Ramesh,
karanamram@gmail.com;
kramesh@ucar.edu

Citation:
Ramesh, K., Smith, A. K., Garcia, R. R., Marsh, D. R., Sridharan, S., & Kishore Kumar, K. (2020). Long-term variability and tendencies in middle atmosphere temperature and zonal wind from WACCM6 simulations during 1850–2014. *Journal of Geophysical Research: Atmospheres*, *125*, e2020JD033579. https://doi.org/10.1029/2020JD033579

Received 22 JUL 2020
Accepted 2 NOV 2020
Accepted article online 18 NOV 2020

Abstract Long-term variability of middle atmosphere temperature (T) and zonal wind (U) is investigated using a three-member ensemble of historical simulations of NCAR's Whole Atmospheric Community Climate Model latest version 6 (WACCM6) for 1850–2014 (165 years). The model reproduces the climatological features of T and U. The contributions of Quasi Biennial Oscillation (QBO) at 10 and 30 hPa, solar cycle (SC), El Niño-Southern Oscillation (ENSO), ozone depleting substances (ODS), carbon dioxide (CO_2), and stratospheric sulfate aerosol (volcanic eruptions) to change in monthly zonal mean T and U are analyzed using multiple linear regression. The signal due to CO_2 increase dominates as a predictor of the net multidecadal global annual mean temperature change at all levels in the middle atmosphere. Contributions from ODS also affect the net multidecadal global mean temperature trend in the stratosphere. Because of similarities in the time evolution of the emissions of CO_2 and ODS, the analysis of existing model output cannot accurately separate the attributions of cooling to these two dominant forcing processes. On shorter time scales, solar flux variations are the largest source of variability in the mesosphere while volcanic eruptions are the largest in the stratosphere. In the stratosphere and mesosphere, both QBO and ENSO can significantly impact zonal mean temperature and zonal-mean zonal wind depending on latitudes, but their impact on the multidecadal global mean temperature trend is very small.

1. Introduction

It is useful to periodically update the assessment of past atmospheric trends to take advantage of increasingly comprehensive global climate models. Understanding of trends ("Trend" in climate usually means changes on a time scale longer than a solar cycle [SC]) in the middle atmosphere (the stratosphere and mesosphere) is particularly dependent on numerical models because the observational record does not extend as far into the past as it does for the lower atmosphere. Middle atmospheric processes are influenced by external forcing (volcanic eruptions and solar UV), anthropogenic composition changes (greenhouse gases and ozone depleting substances [ODSs]), and global impacts of localized tropical variability (QBO and ENSO). Sorting out the impacts of these processes requires accounting for interaction between the ocean and atmosphere and simulation of the chemical feedback on dynamical perturbations. Multiple simulations of the historical climate provide important information for sorting out which patterns and trends are robust and which depend on internal variability in the model.

Numerous previous studies have evaluated the middle atmosphere variability in response to one or more predictors. The predictors are chosen to represent processes that are known or suspected to affect the temperature. The anthropogenic increase of CO_2 and other greenhouse gases affects the radiative budget at all levels of the atmosphere (Akmaev & Fomichev, 1998; Andrews et al., 1987; Gille & Lyjak, 1986; Kuhn & London, 1969; Mlynczak et al., 1999a, 1999b; Mlynczak & Solomon, 1993; Roble & Dickinson, 1989). Ozone loss due to increasing ODSs, composed of chlorine and bromine compounds, influences the temperature by reducing solar heating (e.g., Garcia et al., 2007, 2019; Rowland, 1991). The stratosphere sulfate aerosols resulting from large volcanic eruptions directly affect both incoming shortwave radiation and outgoing longwave radiation (heating and cooling effects) (Robock, 2000) and indirectly affect radiative processes

through transport and chemistry of ozone (Riese et al., 2012; Solomon et al., 2010). The 11-year cycle in solar UV influences the temperature directly and also modifies the composition by photodissociation or excitation of O_2, O_3, and other molecules. The QBO influence is felt through dynamical coupling between the tropical lower stratosphere and the global middle atmosphere; the mechanism may involve wave modulation, circulation changes, and the distribution of chemical species, particularly O_3 and H_2O. ENSO has also been found to have an impact on middle atmosphere temperature, composition, and wave propagation characteristics and circulations (Free & Seidel, 2009; García-Herrera et al., 2006; Li et al., 2013; Manzini et al., 2006; Randel et al., 2009; Sassi et al., 2004).

For middle atmosphere trend studies, numerical models are used in two ways: analyzing output from simulations that include all forcing known or expected to be important (e.g., Garcia et al., 2007, and references therein; Garcia et al., 2016, 2019; Krivolutsky et al., 2015; Li et al., 2013; Lübken et al., 2013; Marsh et al., 2013; Qian et al., 2019; Schmidt et al., 2013) or completing simulations with and without a particular forcing included in order to determine how the simulations differ (e.g., Chiodo et al., 2014).

In addition, observational studies have assessed the variability with the measurements available (e.g., Lee et al., 2010; Sridharan et al., 2009, 2010; Venkat Ratnam et al., 2013, 2019); see the reviews by Beig et al. (2003) and Laštovička (2017). Both simulations and observational analyses are important to improve our understanding of the atmospheric response to the various external and anthropogenic changes that have occurred and are expected to continue.

From the above studies, it is clear that the increasing anthropogenic emissions have great impact on middle and upper atmospheric trends and variability and need to be evaluated in the presence of other processes affecting variability. However, most of the studies cited have one or more of the following limitations: They are based on relatively short simulations, they do not extend beyond 2005, they are confined to specific latitudes and pressure levels, and the analysis may include two or three predictors only. The purpose of the present, comprehensive study is twofold: First, we provide an updated investigation of the long-term variability and tendencies of solar activity, QBO, ENSO, ODS, CO_2, and stratospheric sulfate aerosols and their contributions to changes in middle atmosphere temperature (T) and zonal wind (U), globally. Second, we assess the ability of analysis to provide a clean separation of the relative impacts of different forcing processes. We use three realizations (to enhance statistical reliability) of historical simulations of the National Center for Atmospheric Research's (NCAR) Whole Atmosphere Community Climate Model, Version 6 (WACCM6) for the period of 1850–2014 (165 years). The long-term tendencies in T and U are derived using multiple linear regression (MLR) analysis with seven predictors. Section 2 provides the details of model simulations and data analysis, section 3 presents the results, summary and discussion are elaborated in section 4, and section 5 provides the conclusions drawn from the study.

2. Model Simulations and Methodology

2.1. WACCM6 Simulations

The Whole Atmosphere Community Climate Model (WACCM) is a comprehensive global climate numerical model that extends from the Earth's surface into the lower thermosphere (6×10^{-6} hPa; ~140 km). It is a component of the Community Earth System Model (CESM), a family of models developed at NCAR. The latest version, WACCM6 (Gettelman et al., 2019), is run as the atmospheric component of NCAR's CESM Version 2 (CESM2) (Danabasoglu et al., 2020), and in this configuration it is designated as CESM2 (WACCM6). There are numerous changes to this version from the previous release (WACCM4; Marsh et al., 2013). These include higher horizontal resolution of 0.95° × 1.25° (latitude × longitude) and additional chemical compounds and reactions, including additions to the representation of ion chemistry and heterogeneous reactions. Of particular importance to long-term variability of the middle atmosphere are improved representation of surface drag and orographic gravity waves, an expanded database of volcanic eruptions (Neely & Schmidt, 2016), improved representation of volcanic sulfate aerosols (Mills et al., 2016), representation of secondary organic aerosols (Tilmes et al., 2019), and inclusion of a flux of energetic particles from the space environment (Marsh et al., 2007; Matthes et al., 2017). WACCM6 now simulates a self-generated QBO and an ENSO with realistic magnitude and occurrence rate. The vertical resolution within the middle atmosphere has not changed from the previous version of the model. Vertical resolution varies with altitude as 1.1–1.4 km in the troposphere and lower stratosphere to

1.75 km in the upper stratosphere and 3.5 km in the upper mesosphere and lower thermosphere (Garcia et al., 2017).

In the present study we use an ensemble of three realizations of WACCM6, fully coupled to active ocean and sea ice model components and to an interactive land model, starting from 1850. These simulations were completed as contributions to the Coupled Model Intercomparison Project, Round 6 (CMIP6). Gettelman et al. (2019) give an extensive description of WACCM6, including several important features of the model and its validation. In the present investigation, the archived output of monthly mean temperature and zonal wind from these simulations has been used to study the long-term variability and the responses to the SC, QBO, ENSO, ODS, CO_2, and stratospheric sulfate aerosols in the middle atmosphere for 1850–2014 from all three realizations of the model.

2.2. Analysis Method

2.2.1. Multiple Linear Regression

The regression analysis uses monthly zonal mean output averaged every 3 and 12 months to produce seasonal and annual means, respectively, over the period 1850–2014 at each latitude and pressure grid point. The mean changes are calculated as the difference of the value for each year or season from the average over the period 1850–1860. The regression analysis on the changes in temperature (ΔT) and zonal wind (ΔU) determines the response associated with the SC, QBO, ENSO, ODS, CO_2, and stratospheric sulfate aerosols. This is presented as contributions to changes in T and U in the middle atmosphere from each of these indices, each representing a different forcing.

The standard expression for a MLR model can be given as follows (Chiodo et al., 2014).

$$\Psi(t) = \chi + \sum_{i=1}^{n} C_i K_i(t) + \in (t), \tag{1}$$

where Ψ is the predictand (i.e., the dependent variable, here either T or U), t is time in years, χ is a constant, C_i is regression coefficients corresponding to n predictors, K is a matrix containing n predictors, and $\in$ is the residual. In the present analysis, the matrix K has the following predictors:

$$K = \begin{pmatrix} F_{10.7} \\ QBO10 \\ QBO30 \\ NINO3.4 \\ EESC \\ CO_2 \\ AOD \end{pmatrix}, \tag{2}$$

where

1. $F_{10.7}$ is the solar radio flux at 10.7 cm, a proxy for solar activity (in solar flux units, sfu; 1 sfu = 10^{-22} Wm^{-2} Hz^{-1}). It is specified as a scalar value in these simulations and is identical for the three realizations.
2. *QBO*10 and *QBO*30 are zonal winds (m s^{-1}) averaged over 5°N to 5°S at 10 and 30 hPa, respectively, for QBO. These are calculated from the model self-generated QBO and are different for the three realizations.
3. *NINO*3.4 index is the 3-month running mean of sea surface temperature (K) averaged for 5°N to 5°S and 120–170°W. These values are calculated from the model-generated sea surface temperature and are different for the three realizations.
4. *EESC* is Equivalent Effective Stratospheric Chlorine (ppbv) calculated as the area-weighted global average of the sum of the inorganic chlorine and 60 times the inorganic bromine (ClO_y + 60 BrO_y) at 1 hPa pressure. Here the number 60 accounts for the more efficient ozone depletion by bromine (Newman et al., 2007; Stolarski et al., 2010). The total inorganic chlorine and inorganic bromine are composed of Cl + ClO + $2Cl_2$ + $2Cl_2O_2$ + OClO + HOCl + $ClONO_2$ + HCl + BrCl and Br + BrO + HOBr + $BrONO_2$ + HBr + BrCl, respectively. These values are calculated from

the model output for each realization and have only very slight differences among the three realizations since the emissions of chlorine and bromine compounds are the same in all realizations.

5. CO_2 is the global average of surface carbon dioxide volume mixing ratio (ppmv). This is specified and is identical in the three realizations.
6. *AOD* is the area-weighted global average of stratospheric aerosol optical depth at 550 nm, used as a proxy for stratospheric sulfate aerosols (volcanic eruptions). These values are calculated from the model output and have only slight differences among the three realizations since the emissions from the volcanic eruptions themselves are specified.

The predictors are averaged to get seasonal and annual means, and their changes with respect to 1850–1860 are used in the MLR analysis to compute regression coefficient/response of each predictor. The regression coefficients are then multiplied by the corresponding predictor to derive its contribution for the changes (anomalies) in T or U.

2.2.2. Serial/Auto Correlation Test

The Durbin-Watson (DW) statistic is a test for autocorrelation in the residuals from a statistical regression analysis. The DW test assesses whether or not there is autocorrelation among the residuals of time series data. This is often used to test for positive or negative, first-order serial correlation (the relationship between a variable and a lagged version of itself over various time intervals). It is calculated as follows.

$$DW = \frac{\sum_{t=1}^{n-1} (r_{t+1} - r_t)^2}{\sum_{t=1}^{n} r_t^2}, \tag{3}$$

where r_t is the t^{th} raw residual and n is the number of observations.

The DW statistic value always lies between 0 and 4; a value near 2 indicates no autocorrelation detected in the sample. The values from 0 to less than 2 indicate positive autocorrelation and from 2 to 4 indicate negative autocorrelation. Values between 1.5 and 2.5 are relatively normal; values below 1 and above 3 are causes for concern. In the present study, the DW test has been applied to the residuals from the regression analysis, and it was found that the DW statistic value ranges as 1.5–1.7 for ΔT and 1.9–2.3 for ΔU for the three model realizations. The differences of the DW statistic from 2 indicate that there will be some remaining uncertainties in the conclusions that link certain processes to the changes in the simulated atmosphere. These uncertainties also reflect the simultaneous action of multiple processes in the actual atmosphere.

2.2.3. Statistical Significance

We perform *t* test analysis (see, e.g., Wilks, 2006) to calculate the statistical significance of the responses of ΔT and ΔU to the above mentioned seven regressors (Equation 2). In the figures that follow, the regions where the results are not significant at the 95% confidence level are denoted by stippling in the figures. The test statistic (*t* statistic) is

$$t = \frac{\bar{x} - \mu}{s/\sqrt{n}}, \tag{4}$$

where $\bar{x}$ is the sample mean, μ is the hypothesized population mean, s is the sample standard deviation, and n is the sample size. Under the null hypothesis ($\bar{x} = \mu = 0$), the test statistic has Student's *t* distribution with $n - 1$ degrees of freedom.

3. Results

The results presented in this section show the responses to the seven predictors discussed in section 2. Those that affect only short-term variability and have negligible impact on the longer-term trends are included for completeness. However, the discussion will focus primarily on what we can learn about long-term variations from the WACCM6 simulations.

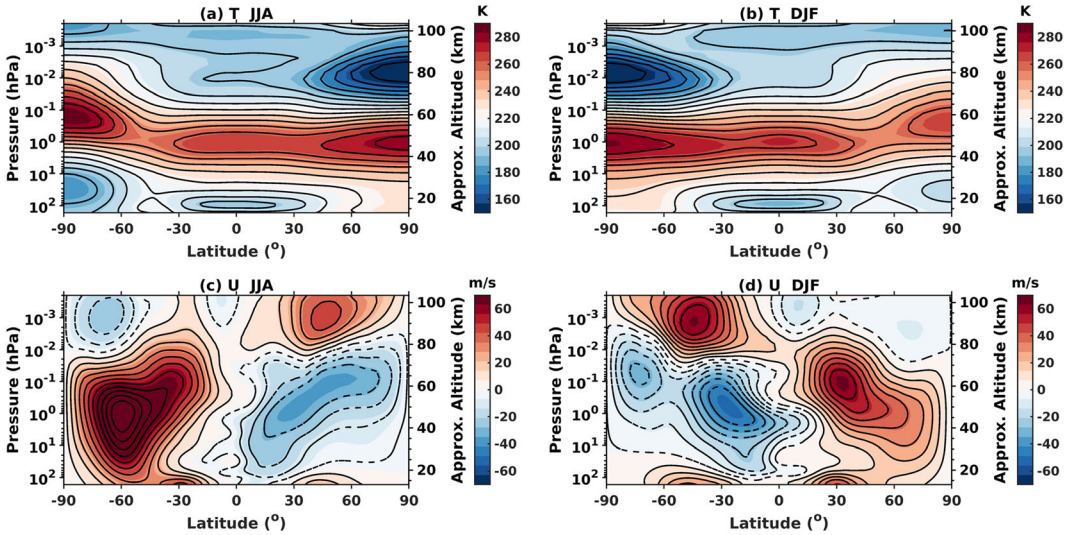

Figure 1. The latitude-pressure variation of composite mean (1850–2014) middle atmosphere (top panels) temperature and (bottom panels) zonal winds for JJA (June—August) and DJF (December–February) averaged for three realizations. Approximate altitudes are given on the right *y* axes.

3.1. Climatology of Temperature and Zonal Wind

Figure 1 illustrates the WACCM6 1850–2014 climatological mean middle atmosphere zonal-mean temperature (top panels) and zonal winds (bottom panels) for JJA (June–August) and DJF (December–February) averaged for the three model realizations. The model reproduces the latitudinal variation of temperature with a colder (~140 K) and lower (~0.006 hPa; ~85 km) summer mesopause and a warmer (~180–190 K) and higher (0.0003 hPa; ~100 km) winter mesopause over the polar regions. The polar stratopause is warmer (~290 K) in summer, located at ~1 hPa (~48 km) in both hemispheres, and tilts upward toward the winter pole, where it is located at ~0.2 hPa (~57 km) with a lower temperature (~265–280 K) in northern winter. The polar winter stratopause is warmer in the Southern Hemisphere (SH; ~285 K) than in Northern Hemisphere (NH; ~265 K).

The atmospheric thermal structure is closely related to the zonal mean wind, which is shown in the lower panels (c and d) of Figure 1 for JJA and DJF. The latitudinal pattern for the solstice periods and the strengths of the jets are well represented in the model. The zonal mean circulation is characterized by westerly (eastward) subtropical jet streams in the troposphere of both the NH and the SH. In the winter hemisphere, westerlies intensify above the tropopause and reach speeds of ~70 m/s in the lower mesosphere (~0.1 hPa; ~60 km). In the summer hemisphere, westerly flow weakens above the tropopause and is replaced by easterly (westward) flow that intensifies up to the mesosphere. Both the winter westerlies and summer easterlies weaken in the upper mesosphere and reverse above ~0.01 hPa (~75 km).

Comparisons of WACCM6 temperature and winds with reanalysis fields were presented by Gettelman et al. (2019). They did not validate the model fields in the upper mesosphere due to lack of observations. Gettelman et al. (2019) note overall good agreement although there are some differences, especially in the zonal winds. The simulated middle atmosphere winds are especially sensitive to the gravity wave parameterization of the model. The impact of possible deficiencies in the gravity wave parameterization on the trends discussed in this paper is not known and constitutes an uncertainty that cannot be evaluated with present-day climate models that must parameterize gravity waves.

3.2. Time Series of Predictors for 1850–2014

The time series of the annual mean predictors used for the regression analysis are shown in Figures 2 and 3 for 1850–2014. The four predictors (defined in section 2.2) shown in Figure 2 are identical, or almost identical, in the three realizations. They represent external ($F_{10.7}$ and aerosol optical depth [AOD] from volcanoes) and anthropogenic (CO_2 and EESC) forcing based on the observational record.

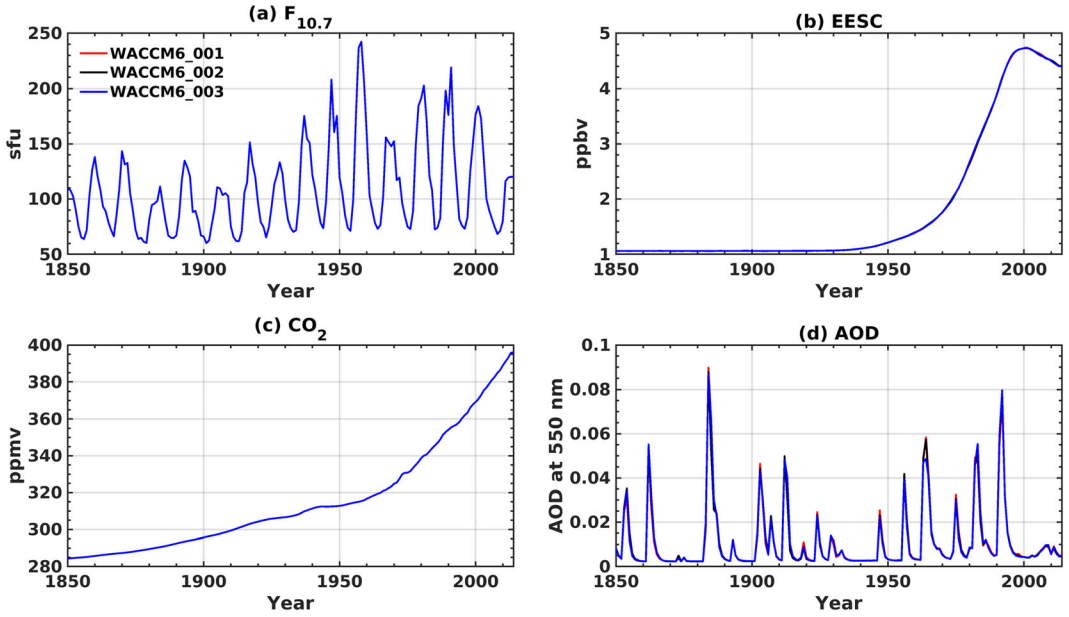

Figure 2. The time series of annual mean predictors, (a, b) $F_{10.7}$ and EESC and (c, d) CO_2 and AOD for three model realizations during 1850–2014.

The time series of QBO10, QBO30, and NINO3.4 indices are shown in Figure 3 for the three realizations. Differences in these indices among the cases are clearly seen. Because of the annual averaging, the QBO10 and QBO30 indices are not large. There are no apparent long-term trends in the QBO indices. The annual average NINO3.4 index is a proxy for ENSO; ENSO events in these simulations are self-generated and are not synchronized among the three simulations. There is a trend in the NINO3.4 index in the most recent decades that is consistent with an overall warming in the ocean temperature.

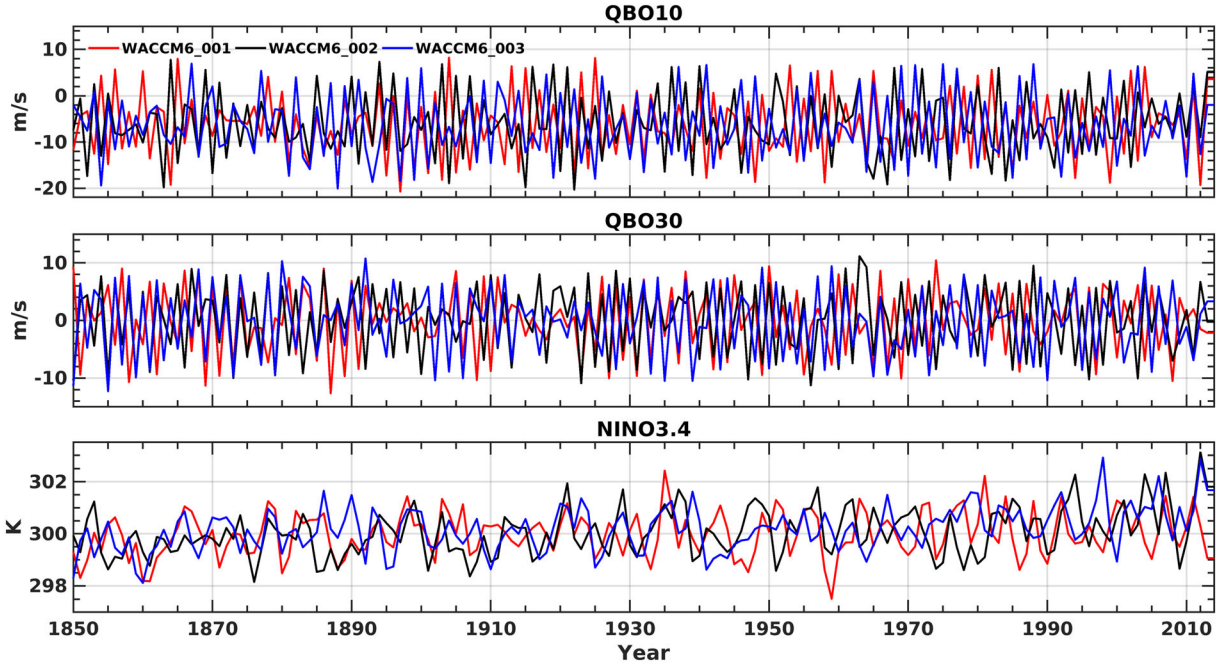

Figure 3. The time series of annual mean predictors, (top) QBO at 10 hPa, (middle) QBO at 30 hPa, and (bottom) NINO3.4 index for three model realizations during 1850–2014.

Table 1
The Correlation Coefficients Among the Regression Terms in Three Model Realizations

$F_{10.7}$	1.0000						
	1.0000						
	1.0000						
QBO10	0.0011	1.0000					
	−0.0242	1.0000					
	−0.0066	1.0000					
QBO30	0.0020	−0.4657	1.0000				
	0.0028	−0.4025	1.0000				
	−0.0040	−0.4331	1.0000				
NINO3.4	−0.0472	−0.0729	0.0687	1.0000			
	0.1432	−0.0156	−0.0278	1.0000			
	0.1014	−0.0723	−0.0443	1.0000			
EESC	0.1967	0.0414	0.0023	0.0880	1.0000		
	0.1959	0.0698	−0.0326	0.3384	1.0000		
	0.1966	0.0049	−0.000308	0.4127	1.0000		
CO_2	0.2439	0.0451	−0.0063	0.1178	0.9445	1.0000	
	0.2439	0.0835	−0.0188	0.3917	0.9444	1.0000	
	0.2439	0.0136	−0.0148	0.4414	0.9442	1.0000	
AOD	0.0342	−0.0488	0.000327	0.1222	0.0578	0.0248	1.0000
	0.0326	−0.0334	0.0255	0.0420	0.0580	0.0200	1.0000
	0.0283	−0.0609	0.0656	0.0235	0.0610	0.0208	1.0000
	$F_{10.7}$	QBO10	QBO30	NINO3.4	EESC	CO_2	AOD

Note. Text in red = WACCM6_001; text in blue = WACCM6_002; text in black = WACCM6_003.

The correlation coefficients among the regression predictors are given in Table 1. Values below 0.05 are indistinguishable from zero. The predictors are approximately independent (values are below 0.5) except between EESC and CO_2. Due to the high correlation between these two indices, which stems from their rapid growth in the second half of the 20th century, the MLR analysis may not correctly attribute the process that is forcing trends in the model; see section 3.6. Also note that the correlation of NINO3.4 with CO_2 and EESC for two of the realizations is in the range 0.3–0.5. This indicates that there may be some ambiguity in attribution of forcing involving ENSO as well.

3.3. Global and Annual Mean Temperature Change

The regression model described in section 2.2 has been applied to annual global mean temperature changes (ΔT) as a function of time (year) for each pressure level. The regression model was applied separately to the output of each realization because of the differences in T and in the phases of QBO10, QBO30, and NINO3.4 indices (Figure 3) among the three model realizations. The contribution of each index to the net change in T with respect to 1850–1860 has been calculated through the product of regression coefficient and the corresponding index and then averaged for all the three realizations for presentation. Here we compare the time series of temperature change associated with the seven predictors for four pressure regions: the lower (10.7–103.3 hPa) and upper (0.95–10.7 hPa) stratosphere in Figure 4 and for the lower (0.01–0.95 hPa) and upper (0.0002–0.01 hPa) mesosphere in Figure 5. Averaging was carried out using all model levels within the range without pressure weighting. As noted earlier, temperature perturbations are shown as changes with respect to the average over the period 1850–1860.

The top panels of Figure 4 indicate that the temperature with respect to 1850–1860 decreases with time in the stratosphere at a rate that is faster in the upper stratosphere (net change of −5.5 K) than in the lower stratosphere (−2.5 K). The rate of temperature decrease is comparatively small until 1950 in both regions (−0.25 K/decade), and then it accelerates after 1950 (to −0.7 K/decade in the upper stratosphere). The long-term change of stratospheric temperature is associated with the cooling influences of CO_2 and the ozone loss associated with EESC. The large irregular variations in the lower stratosphere are associated with aerosol effects from volcanic eruptions. The SC influence is fairly weak in the lower stratosphere but is larger in the upper stratosphere. The QBO signals do not have major effects on the annual global mean stratospheric temperatures while the contribution due to ENSO shows a long-term increase of about 0.1 K.

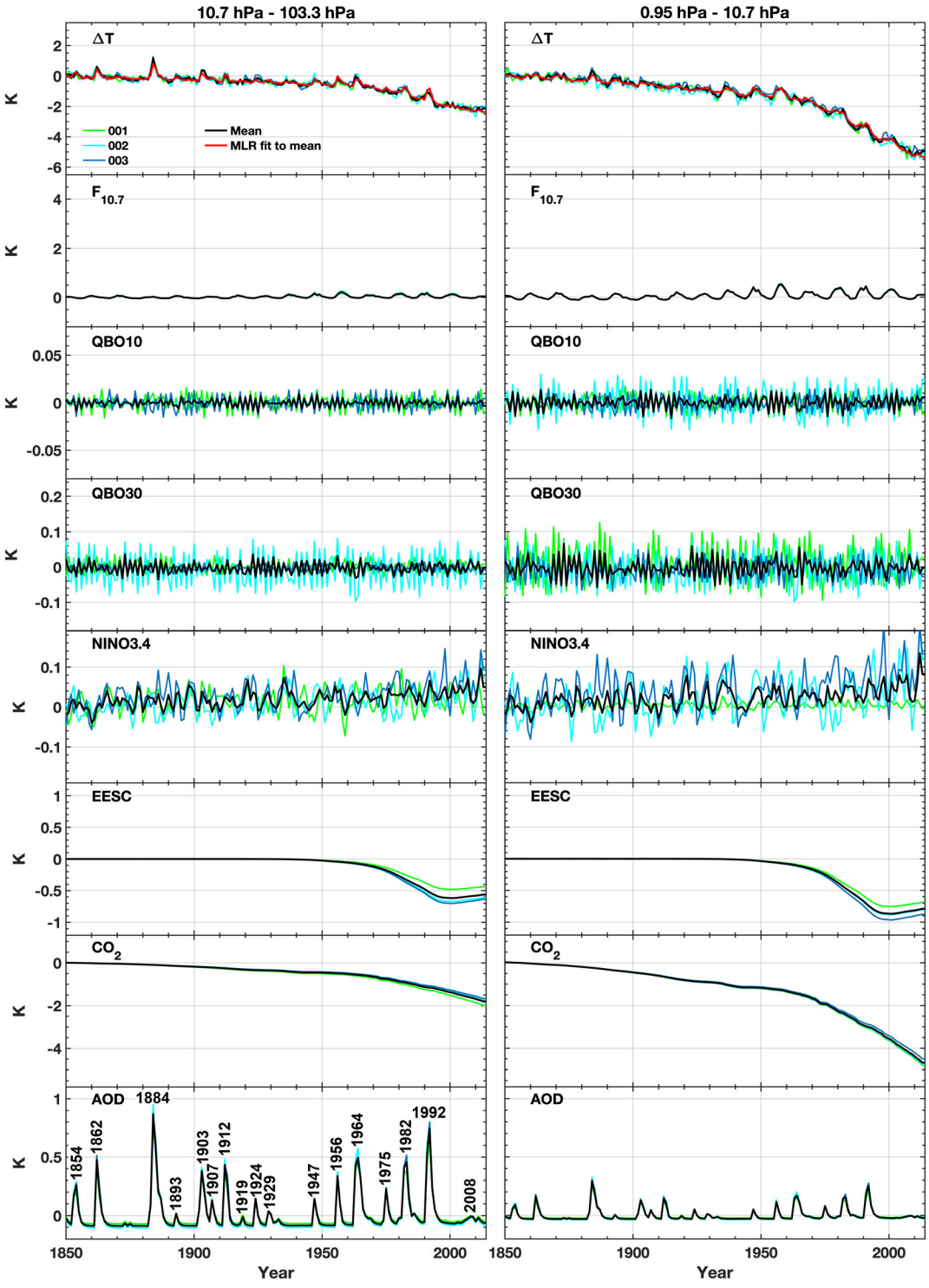

Figure 4. The temporal variation of annual mean and area weighted global mean ΔT with MLR fits to mean of three realizations (001, 002, and 003) and the contribution of each index, namely, $F_{10.7}$, QBO10, QBO30, NINO3.4, EESC, CO_2, and AOD averaged for (left panel) lower stratosphere (10.7–103.3 hPa) and (right panel) upper stratosphere (0.95–10.7 hPa).

Figure 5 shows that the magnitude of the temperature decrease in the mesosphere is faster in the lower (−6.5 K by 2014) than the upper (−5 K by 2014) mesosphere. This difference reflects the relative magnitudes of the CO_2 influence in the two regions. In the upper mesosphere, the MLR analysis attributes a warming

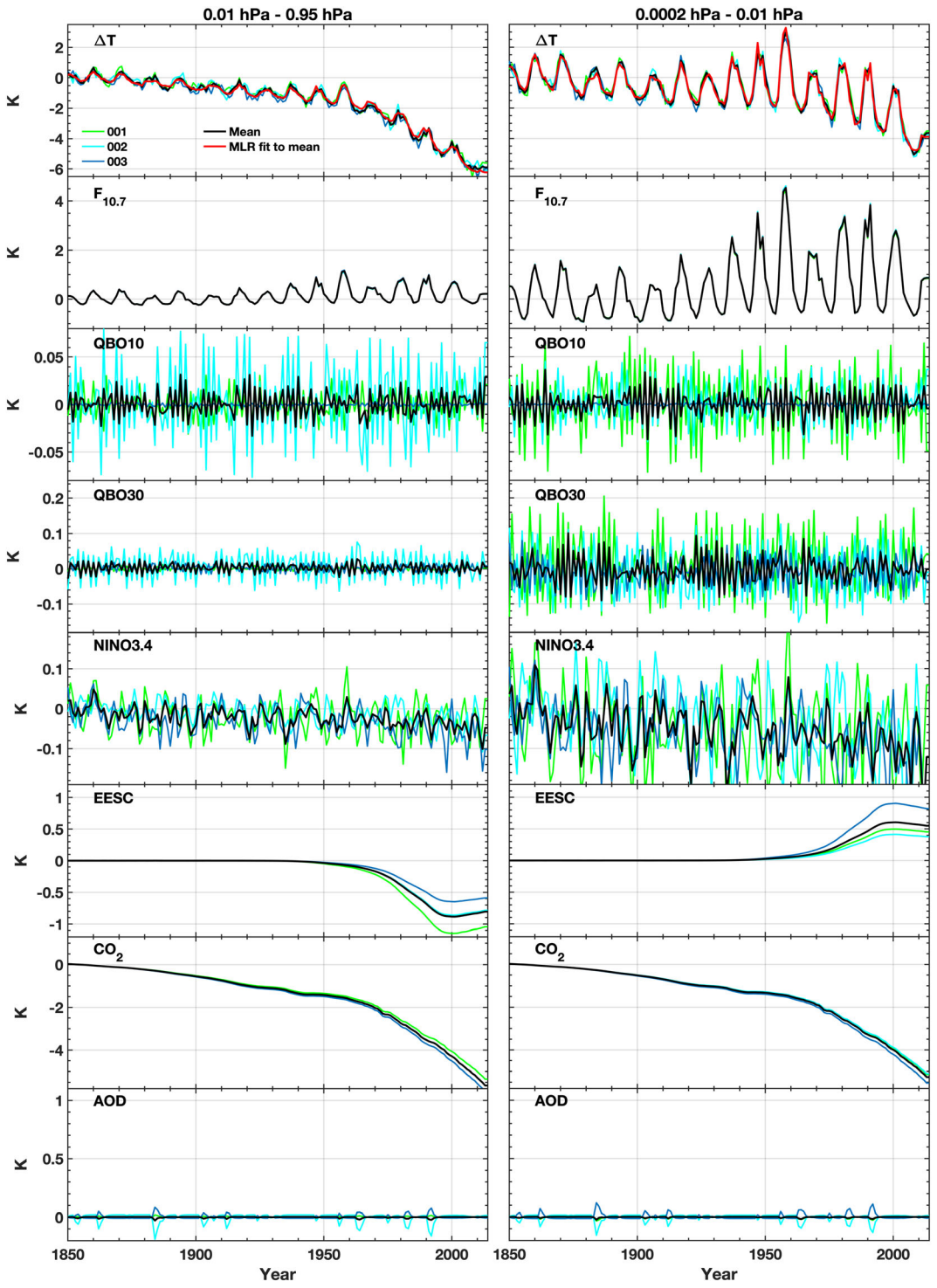

Figure 5. The same as Figure 4 but averaged for (left panel) lower mesosphere (0.01–0.95 hPa) and (right panel) upper mesosphere (0.0002–0.01 hPa).

contribution to the long-term change to EESC that partially cancels the impact of the CO_2 cooling. Here it is worth noting that the net change in temperature (cooling) in the upper mesosphere is slightly smaller than that in the upper stratosphere (Figure 4) and lower mesosphere. The impact of the 11-year SC signal is

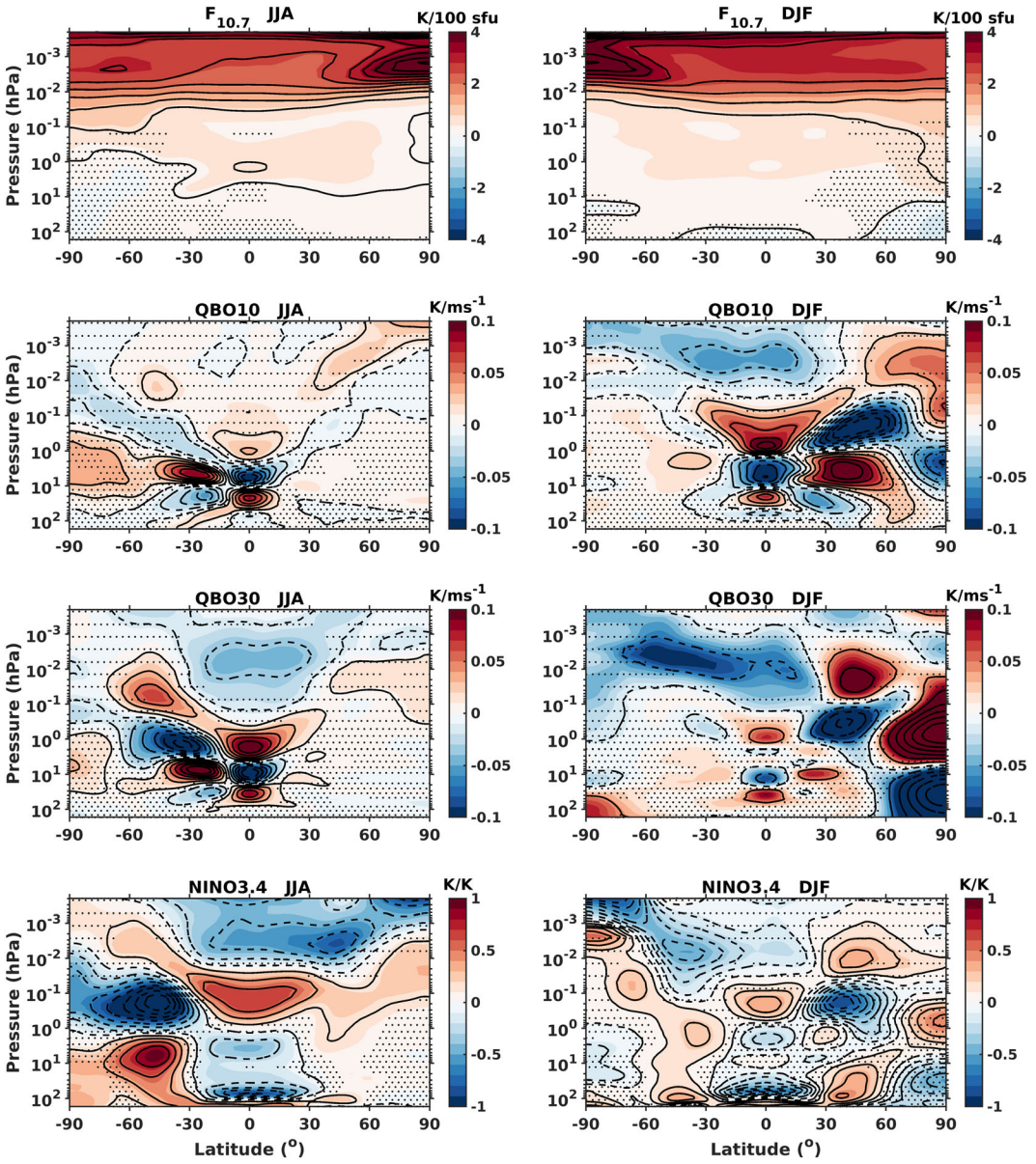

Figure 6. The latitude-pressure distribution of ΔT responses to $F_{10.7}$, QBO10, QBO30, and NINO3.4 index for (left panel) JJA and (right panel) DJF. The responses in stippled regions are not significant at the 95% confidence level ($p > 0.05$).

evident in the lower mesospheric ΔT and even stronger in the upper mesosphere. The volcanic signals have minimal impacts on the temperature change. The EESC signal is apparent into the upper mesosphere even though ozone loss due to halogen chemistry is negligible there; see the discussion in section 3.6.

3.4. Latitudinal Distribution of Temperature Response

Figures 6 and 7 show the latitude-pressure dependency of the temperature changes on the seven predictors for JJA and DJF averaged for the three realizations. The solar response is positive and more significant in the upper mesosphere above ~0.01 hPa with strong heating in the summer polar mesopause region. The QBO10 and QBO30 responses indicate the strongest temperature responses in the equatorial and low-latitude regions, as expected; however, there are also strong responses in midlatitude regions during winter. The response to NINO3.4 shows a similar alternating positive and negative pattern in the tropics during the two seasons shown. However, the summer and winter hemispheres differ even over the limited regions where the signals are significant.

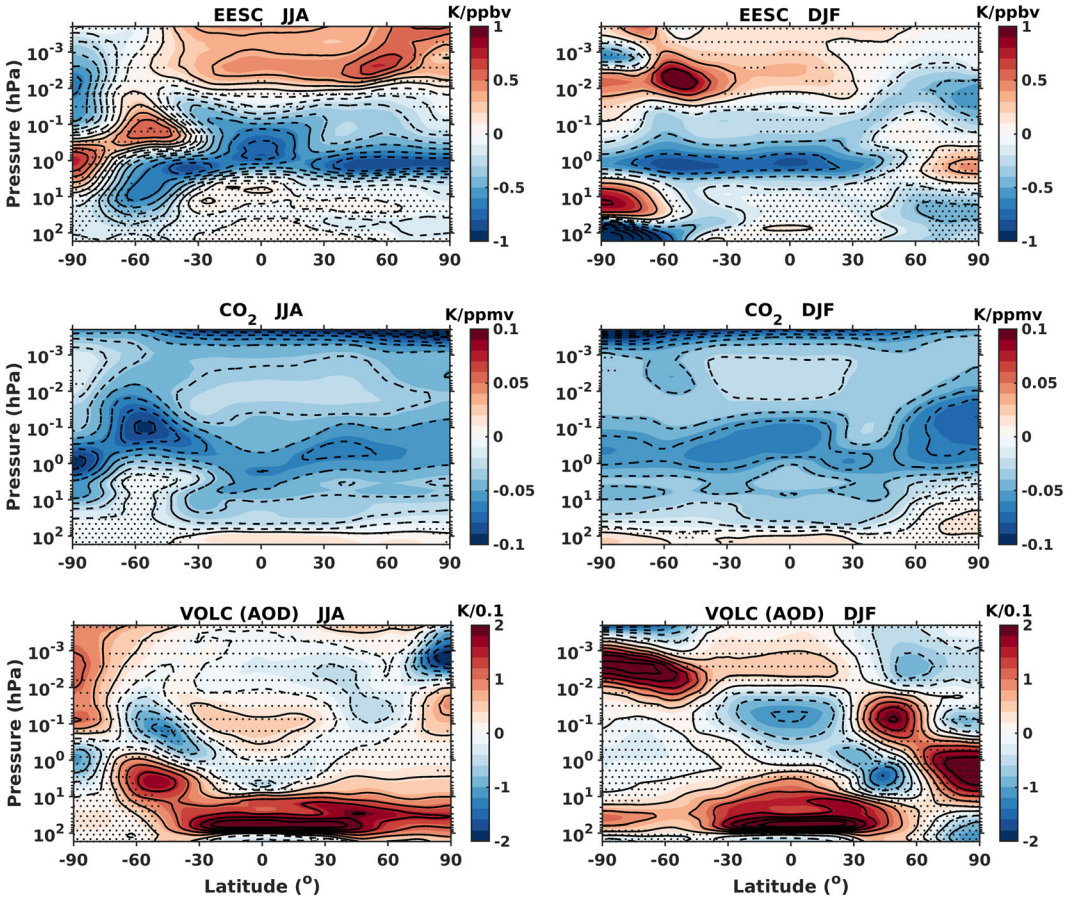

Figure 7. The latitude-pressure distribution of ΔT responses to EESC, CO_2, and AOD for (left panel) JJA and (right panel) DJF. The responses in stippled regions are not significant at the 95% confidence level ($p > 0.05$).

The response to EESC (Figure 7) is negative and reaches a value of −1 K/ppbv in the stratopause (~1 hPa) region in the summer hemisphere and low-latitude and midlatitude winter hemisphere. The strong cooling in the lowermost stratosphere is overlaid by strong heating in the Antarctic polar cap (60–90°S) in DJF. The heating is a dynamical response to the underlying radiative cooling due to ozone loss (Solomon et al., 2017). As also seen in Figure 5, there is a positive EESC response in the upper mesosphere.

The CO_2 response is negative throughout the middle atmosphere and indicates significantly stronger cooling in the stratopause region and above the mesopause. It is largest (around −0.1 K/ppmv) in the winter polar stratopause region. The largest apparent cooling per unit of (surface) CO_2 occurs in the winter high latitudes where the local CO_2 concentration is low due to the downwelling mean circulation. This is an indication of the interpretation challenges introduced by using a single index globally rather than a local predictor for each specific latitude, pressure, and month. On the other hand, a local predictor would not allow for a clear understanding of how the temperature response varies with time.

The stratospheric aerosol (volcanic) signals are expressed with respect to a global mean AOD signal of 0.1 (Schmidt et al., 2013). The response is positive (2 K/0.1 AOD) with strong heating in the lower stratosphere over low latitudes. The heating further extends to the summer pole and parts of winter midlatitudes. In addition to direct radiative forcing, the volcanic aerosols that penetrate into the stratosphere influence the Brewer-Dobson circulation (Diallo et al., 2017), which affects the concentration of water vapor and ozone (Riese et al., 2012; Solomon et al., 2010) and thereby the temperature (e.g., Hansen et al., 1996; Tilmes et al., 2011). The net poleward transport due to the Brewer-Dobson circulation in the stratosphere allows the aerosols to spread globally (e.g., Oman et al., 2005). However, in winter, large-scale subsidence removes some of the stratospheric aerosols over the polar regions (Andersson et al., 2015) and thus reduces the

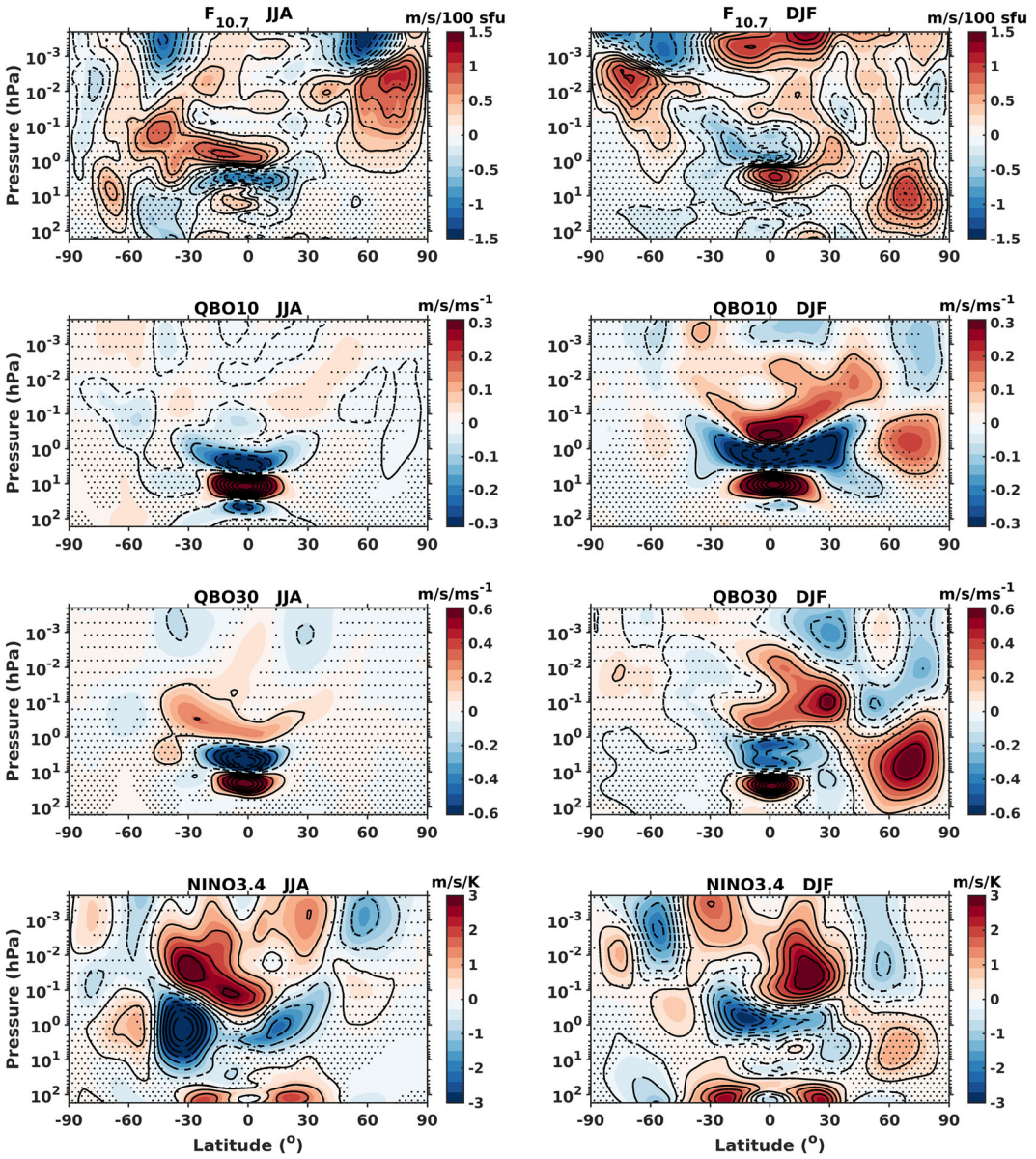

Figure 8. The latitude-pressure distribution of ΔU responses to $F_{10.7}$, QBO10, QBO30, and NINO3.4 index for (left panel) JJA and (right panel) DJF. The responses in stippled regions are not significant at the 95% confidence level ($p > 0.05$).

heating. Due to the weaker long wave radiation and lower solar insolation over the middle and high latitudes, the aerosol heating over these latitudes is comparatively smaller than that over the tropics. The volcanic aerosol signal is insignificant in most parts of the mesosphere.

3.5. Latitudinal Distribution of Zonal Wind Response

The zonal winds are related to temperature gradients in approximate agreement with the thermal wind balance (Andrews et al., 1987); the precise balance can vary since it is also affected by the strong dynamical forcing in the middle atmosphere. We present the long-term variability in the middle atmosphere zonal wind using the regression analysis. Wind observations from ground-based and orbiting platforms provide important information about the middle atmosphere. The model results in this section provide some guidance about the forcings that affect the winds that might be helpful in interpreting the winds from either observations or simulations.

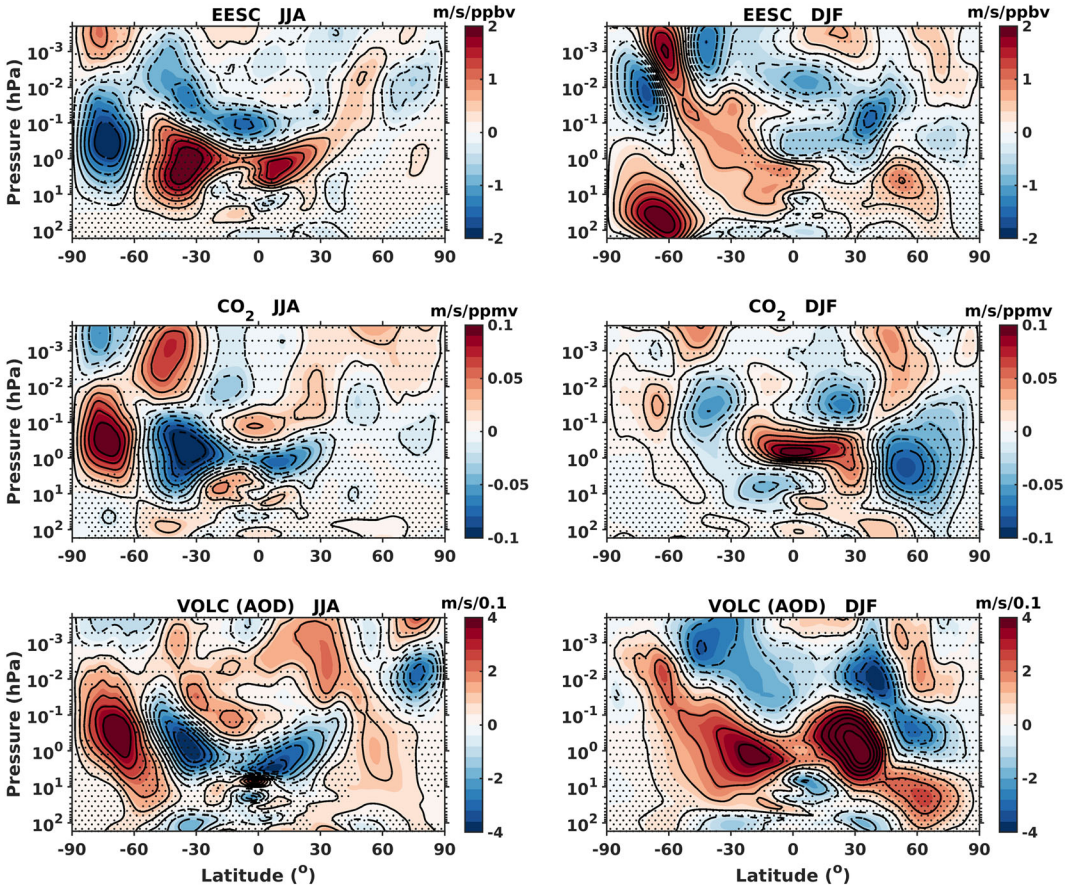

Figure 9. The latitude-pressure distribution of ΔU responses to EESC, CO_2, and AOD for (left panel) JJA and (right panel) DJF. The responses in stippled regions are not significant at the 95% confidence level ($p > 0.05$).

The latitude-pressure variations of the ΔU response are shown in Figures 8 and 9 for JJA and DJF averaged for three realizations. It is evident that the signals show reduced areas of significance compared to the corresponding temperature responses. However, a few features appear to be robust. The responses that are strong and significant (e.g., the response to CO_2 in the SH during JJA) often are seen as a positive and negative pair. Such a pattern can represent movement of a jet in latitude and/or in pressure. In the case of CO_2 in JJA, it indicates a poleward shift of the westerly winter jet as the CO_2 has increased.

Each of the indices has at least some region where the signal is significant. However, due to the limited regions of significance, we will not discuss the individual features. One pattern to note is that the response to EESC and CO_2 in the SH during JJA have similar structures but opposite signs. Considering the net change in the indices since preindustrial times, the magnitudes of these two are comparable, on the order of ~10 m/s, so there is some cancelation between them. In other words, the analysis indicates that the CO_2 increase suggests a poleward movement of the SH winter jet while the ozone loss due to increasing EESC suggests an equatorward movement. As discussed in the following section, there is reason to believe that the MLR analysis has some difficulty distinguishing the responses to these two forcings; this may contribute to the apparent cancelation.

3.6. Correlated Predictors and Variance Inflation Factor

In regression analysis, if one independent variable is correlated with another, there exists multicollinearity which inflates the variances of the parameter estimates and hence might lead to lack of statistical significance of individual predictors. This has been noted previously for shorter time series where correlation of ENSO with the SC (Marsh & Garcia, 2007) or of volcanic eruptions with the SC (Chiodo et al., 2014) was

Table 2
Variance Inflation Factors (VIF) for the Seven Predictors in Three Model Realizations

Parameter	$F_{10.7}$	QBO10	QBO30	NINO3.4	EESC	CO_2	AOD
VIF (Included all)	1.0868	1.2870	1.2817	1.0534	9.5803	9.8579	1.0343
	1.0821	1.2143	1.2027	1.2062	9.6676	10.3258	1.0203
	1.0770	1.2498	1.2443	1.2624	9.4865	9.9642	1.0233
VIF (No CO_2)	1.0460	1.2862	1.2808	1.0340	1.0556	—	1.0213
	1.0489	1.2036	1.1953	1.1411	1.1692	—	1.0058
	1.0411	1.2489	1.2441	1.2246	1.2490	—	1.0097
VIF (No EESC)	1.0460	1.2868	1.2808	1.0340	—	1.0556	1.0213
	1.0489	1.2036	1.1953	1.1411	—	1.1692	1.0058
	1.0411	1.2489	1.2441	1.2246	—	1.2490	1.0097

Note. Text in red = WACCM6_001; text in blue = WACCM6_002; text in black = WACCM6_003.

shown to affect the interpretation. Those particular correlations are not a problem for our very long time series. Nevertheless, because of the high correlation (~0.9) observed between EESC and CO_2 indices (Table 1), we look further at the impact of correlations in predictors on the analysis results.

We calculate the variance inflation factor (VIF), which is widely used to diagnose the degree of multicollinearity in a multiple regression (e.g., Miles, 2014; O'brien, 2007). It is calculated for the ith predictor as $VIF_i = 1/(1-R_i^2)$, where R_i is the coefficient of determination. As a rule of thumb, multicollinearity is a potential problem when $VIF_i > 10$ (e.g., Kutner et al., 2004). Table 2 illustrates the VIF value of each predictor anomaly (annual mean) for the three realizations. The values are around 1 for all the predictors except for EESC (~9.4–9.6) and CO_2 (~9.8–10.3). Since the VIF values for EESC and CO_2 are close to 10, we look further into the use of these two predictors. The MLR analysis described in section 2.2.1 is repeated twice: once using all predictors except CO_2 ("no CO_2") and the second time using all predictors except for EESC ("no EESC"). The VIF values for both of these cases are significantly improved and are in the range of 1.0–1.3 for all the predictors.

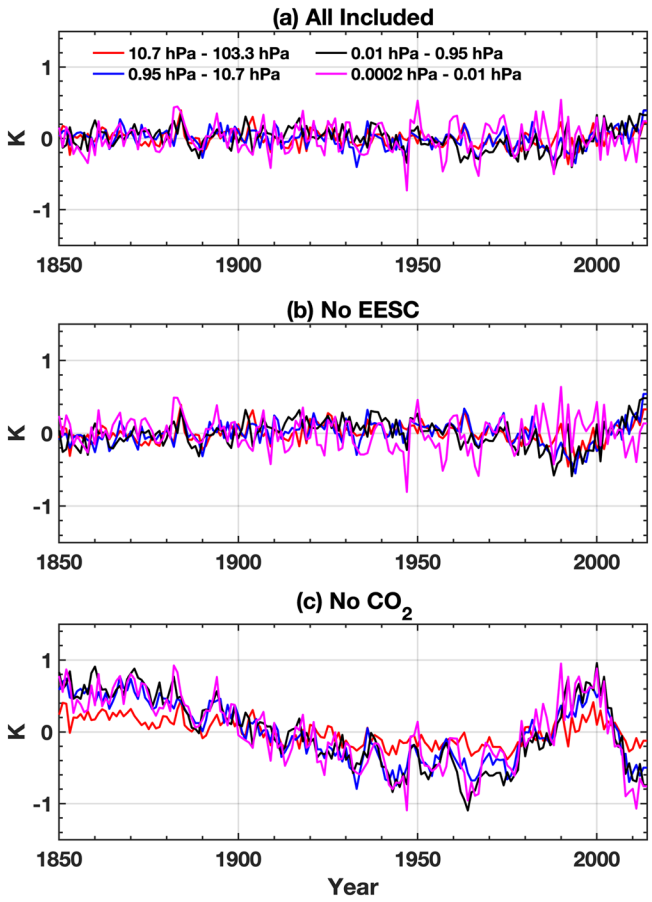

Figure 10. The temporal variation of annual mean and area-weighted global mean differences between mean ΔT and the corresponding MLR fit when (a) all the predictors included, (b) EESC removed, and (c) CO_2 excluded in the regression analysis for the stratosphere and mesosphere.

Figures 10a–10c show the differences between mean ΔT and the corresponding MLR fit when (a) all the predictors are included, (b) EESC is omitted, and (c) CO_2 is omitted in the regression analysis for the stratosphere and mesosphere. It is evident that the differences stay within the limit of ±0.5 K at all pressure ranges when all predictors are included. When the EESC is excluded (Figure 10b), there are no abrupt changes in the differences between the model's ΔT and the MLR fit. The differences remain similar to that of the "all included" case up to about 1980, after which they are larger and more variable but still remain below ~0.6 K in magnitude. The changes in the no-EESC case are most prominent in the upper stratosphere and lower mesosphere and indicate a sharp rise toward the end of the 20th century when the trend in EESC diverges from that of CO_2 (Figure 2). When CO_2 is omitted from the analysis (Figure 10c), the differences reach magnitudes of ±1 K. Even though there is a high correlation of the CO_2 and EESC indices, the comparison in Figure 10c shows that EESC, in combination with other indices, cannot adequately compensate for the omission of the CO_2 predictor.

The omission of either CO_2 or EESC as a predictor leads primarily to the other index "predicting" the bulk of the long-term changes that were previously "explained" by the removed index. To illustrate this, Figure 11 shows the time series of annual mean and area-weighted global mean contributions for the temperature change with respect to 1850–1860 due

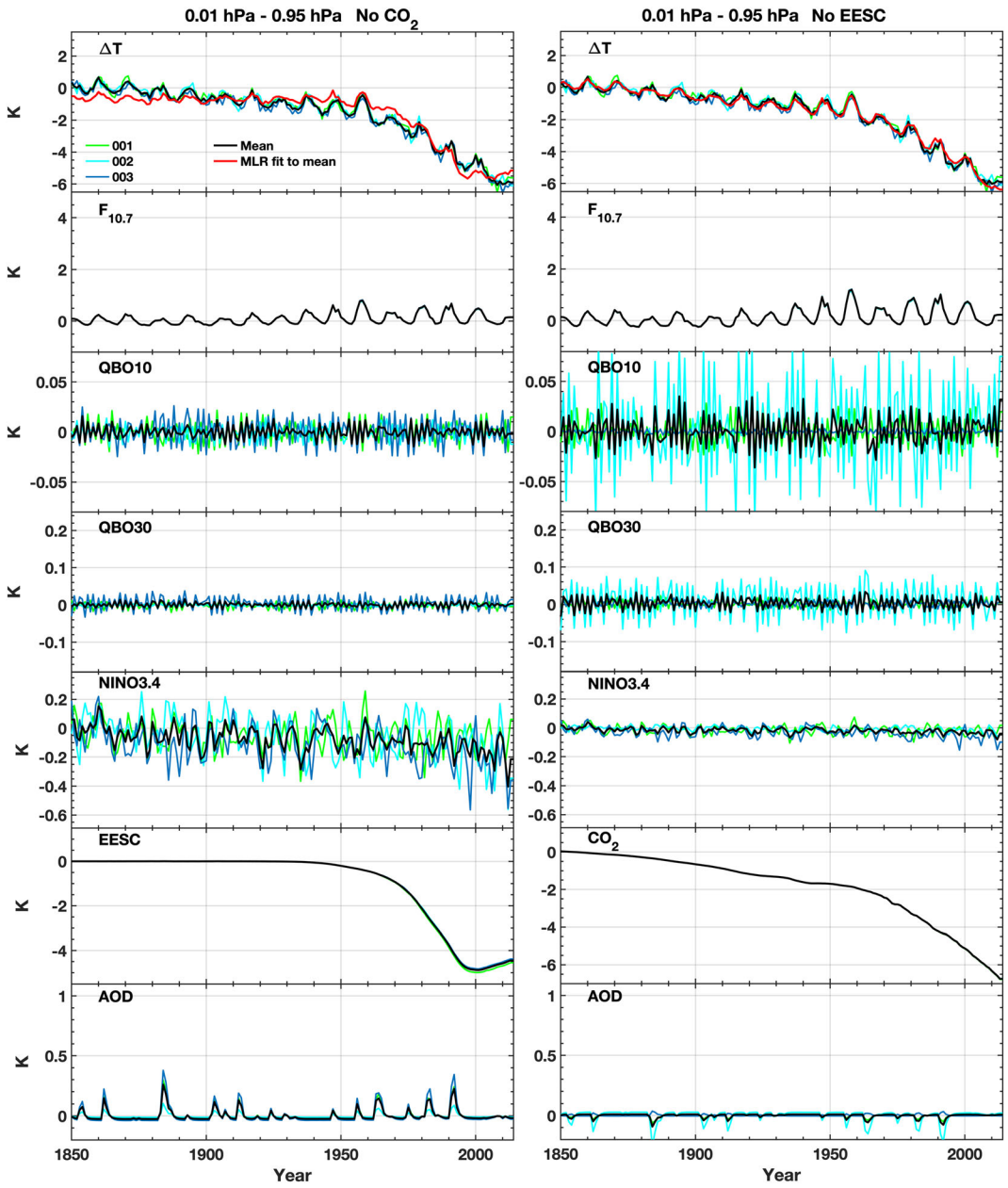

Figure 11. The temporal variation of annual mean and area weighted global mean ΔT with MLR fits to mean of three realizations (001, 002, and 003) and the contribution of the predictors averaged for the lower mesosphere (0.01–0.95 hPa) when (left column) CO_2 removed and (right column) EESC excluded in the regression analysis.

to all the predictors in the lower mesosphere (0.01–0.95 hPa) for the cases "no CO_2" (left column) and "no EESC" (right column). The contributions shown in this figure can be compared directly with that shown in Figure 5 (left column), which includes all the seven predictors simultaneously in the MLR analysis.

This can be directly compared to the panels in the left column of Figure 5. It is clear from Figures 10 and 11 that the deviation of the MLR fit from the mean ΔT is relatively larger when CO_2 is excluded. The role of several of the predictors changes: EESC exhibits maximum cooling of up to −4.5 K (in 1995), the AOD signal shows heating of up to 0.4 K, and the net cooling due to NINO3.4 increases slightly by −0.4 K. The "no-CO_2" case also suggests an increase in the response of the mesosphere to AOD (lower left panel of Figure 11), but this is not significant. For the case of "no EESC," most of the signals remain the same, except that the net

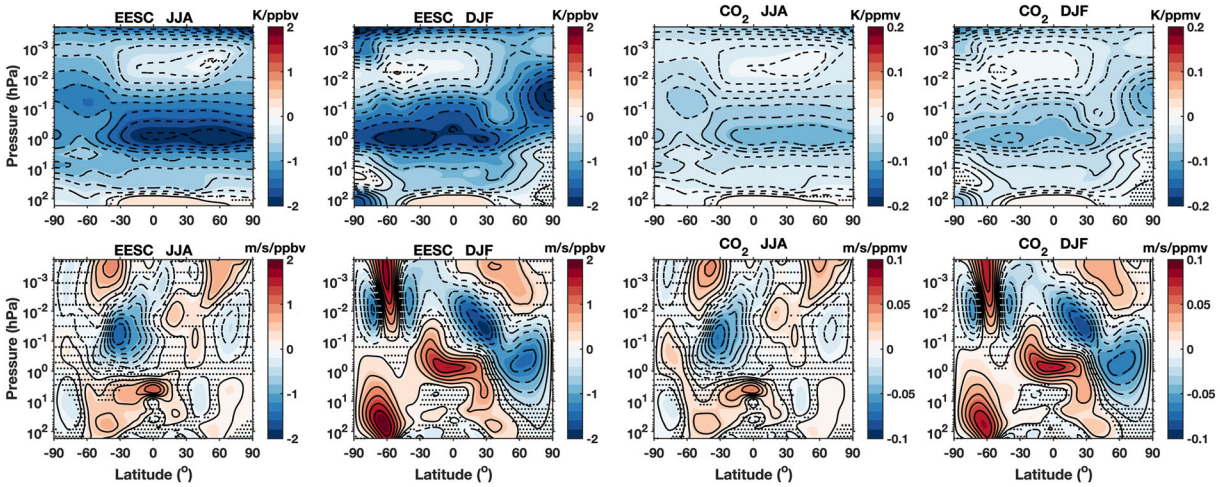

Figure 12. The latitude-pressure distribution of (top) ΔT and (bottom) ΔU responses to EESC and CO_2 for JJA and DJF when (left two columns) CO_2 is omitted and (right two columns) EESC is omitted in the regression analysis. The responses in stippled regions are not significant at the 95% confidence level ($p > 0.05$). The contour intervals for panels in the top row are twice those in the corresponding plots of Figure 7.

cooling that is attributed to CO_2 increases by up to 7 K (vs. about 6 K in the full MLR; Figure 5, right column). In contrast to what is shown in Figure 5, in the absence of a CO_2 predictor, the response to the EESC forcing shows cooling instead of heating in the upper mesosphere (not shown).

The latitude-pressure distribution of ΔT and ΔU responses to EESC and CO_2 for JJA and DJF is shown in Figure 12 for "no CO_2" (left two columns) and "no EESC" (right two columns). It is worth noting that, in both the "no-EESC" and "no-CO_2" cases, the responses due to $F_{10.7}$, QBO10, QBO30, NINO3.4, and AOD remain almost unchanged and are similar to that shown in Figures 6–9 for both ΔT and ΔU (not shown). The ΔT responses to EESC ("no CO_2") and CO_2 ("no EESC") are similar to each other in the entire middle atmosphere in JJA and DJF. Although there are no appreciable changes in CO_2 cooling, the cooling that is attributed to EESC doubles (up to −2 K) at the stratopause region and is negligible (instead of heating, as indicated in Figure 7) around the mesopause in the summer hemisphere, including winter low latitudes. Similarly, the ΔU response to EESC ("no CO_2") and CO_2 ("no EESC") are analogous to each other in the entire middle atmosphere in JJA and DJF. In contrast to that shown in Figure 9, the oppositely signed strong westerly and easterly jets due to EESC and CO_2 are absent in the SH high latitude upper stratosphere and lower mesosphere in JJA.

The results in this subsection illustrate the importance of the set of predictors used in the analysis when seeking to attribute long-term changes to particular sources. In the analysis throughout this investigation, we have used two predictors (CO_2 surface concentration and averaged EESC in the stratosphere) that are assumed to capture the bulk of the net long-term composition changes over 165 years. Furthermore, we have assumed that the response of the middle atmosphere temperature to those and other varying predictors is linear. However, a more careful look at the relative roles of these two indicators of evolving composition indicates that the analysis of time series data when both processes are present is not able to distinguish their impacts. Although we use MLR analysis for this investigation, the attribution problem documented here is not confined to that technique. Rather, it reflects the simultaneous growth and temporal correlation of the anthropogenic gases that contribute to the two indices.

4. Summary and Discussion

The present study has investigated the long-term variability and tendencies of the middle atmosphere temperature and zonal winds for the 165-year period 1850–2014, and the contributions to these long-term variabilities by the SC ($F_{10.7}$), QBO at 10 and 30 hPa, ENSO (NINO3.4), ODSs (EESC), CO_2, and stratospheric volcanic aerosols (AOD), through MLR analysis of NCAR's WACCM6 model output. We look at the

analysis results from several different perspectives. First, we examine how the changes in the annual global mean temperature are predicted by the seven indices just mentioned. These are presented as time series over the entire 165-year period averaged over four different pressure ranges. Then we look at the seasonal regression coefficients for 3-month averages at both solstice periods as functions of latitude and pressure. The latter are shown for both temperature (Figures 6 and 7) and zonal wind (Figures 8 and 9).

The model simulations support previous studies showing that the global and annual mean temperature in the stratosphere and mesosphere has decreased with respect to preindustrial time, initially at a slower rate up to 1950 and more rapidly afterward. MLR analysis indicates that the global-average temperature trend is mainly related to the rapid increase of both EESC and CO_2 after 1950. Near the stratopause, the cooling due to EESC growth increases strongly from 1950 to 1995 and then decreases slowly. Absorption of solar ultraviolet radiation (200–450 nm) by ozone is the major heat source in the stratosphere; the cooling tendency of EESC can be attributed to the ozone depletion. The EESC has a negligible impact on O_3 in the upper mesosphere. Akmaev (2012) and Akmaev et al. (2006) interpreted the mesospheric response to stratospheric ozone loss as an indication of thermal contraction. However, our analysis shows that analysis may give incorrect relative attributions to EESC and CO_2 forcing because of the high correlation between their growth rates. Because of this, we would like to focus on the uncertainty in the attribution of the trend rather than on the interpretation of the physics behind individual contributions.

On shorter timescales, the stratospheric temperature changes are also influenced by ENSO and volcanic aerosols (H_2SO_4) and to a lesser extent by solar flux and QBO. There is also a long-term response to NINO3.4, evident as a weak warming tendency in the stratosphere when the index is positive. The magnitude of this response, like that of the response to CO_2, increases after 1950. The trend in the ENSO temperature response could be due to the combined effect of the ENSO perturbations to water vapor (cooling) and ozone (heating) in the stratosphere (Marsh & Garcia, 2007; Solomon et al., 2010). The stratospheric aerosols from large volcanic eruptions contribute a heating tendency by absorbing incoming solar radiation and outgoing infrared radiation and, as a result, contribute net heating in the lower stratosphere (e.g., Diallo et al., 2017; Mehta et al., 2015, and references therein). The heating by volcanic aerosols is comparatively smaller in the upper stratosphere due to their low abundance there.

In addition to temperature, the zonal wind responses to the seven predictors for JJA and DJF are also presented in this paper. Away from the equator, the zonal wind and temperature changes are roughly consistent in accordance with the thermal wind relation. Although some of the model trends and variations, such as the cooling associated with increases in CO_2, are driven by radiative processes, in general it is not possible in a study such as this to attribute each response solely to thermodynamics or dynamics. The zonal wind changes are less often significant than those of temperature. An extensive body of work indicates that variable wave driving plays a leading role in the middle atmosphere responses to the QBO and ENSO.

We would like to emphasize the conceptual ambiguity introduced with collinearity in the regression model. In the present study, the multicollinearity has been tested using the VIF and found that it is approximately equal to 1 for all the predictors except for EESC and CO_2, whose values are nearly equal to 10. To test the effect of collinearity in the MLR, the regression coefficients were calculated while omitting either EESC or CO_2. These calculations indicate that the responses of ΔT and ΔU to $F_{10.7}$, QBO10, QBO30, and NINO3.4 are not affected significantly. Although there are appreciable differences in the EESC and CO_2 signals, there is a similarity in the latitude-pressure domain in that both indicate maximum cooling in the stratopause region. Due to the correlation of these two indices, care must be taken in interpreting the analysis since it is not possible to determine precisely the relative importance of CO_2 and EESC increases on the middle atmosphere temperature changes since preindustrial times. We emphasize that this inability to separate the impacts of these two major drivers of middle atmosphere trends occurs despite the very long record (1850–2014) used in these simulations.

5. Conclusions

The conclusions from this study can be summarized as follows.

1. Using three long simulations and an updated model confirms from previous studies that increases in CO_2 and ODSs have contributed to cooling in the middle atmosphere.

2. The multidecadal historical simulations provide new information about variations in the pace of the changes at different levels. The temperature decreases (cooling) globally with respect to preindustrial times (1850–1860) at a relatively faster rate in the upper stratosphere and lower mesosphere than in the regions above or below during 1850–2014. The long-term temperature changes are not well represented as linear decreases.
3. Another new finding from the extended simulations is the evolution of the relative impacts of various perturbations through the years. The primary predictors that impact the long-term net global annual mean temperature changes are CO_2 and ODSs (represented by EESC); ENSO also makes a minor contribution.
4. For shorter-term variations, volcanic aerosols and ENSO contribute in the stratosphere while the SC contributes in the mesosphere. The effect of QBO on the annual global mean temperature is small.
5. Using multiple simulations with self-generated QBO and ENSO ensures less correlation between these indices and other interannual signals; such correlations have affected interpretation of the drivers of variability in earlier studies. Seasonal responses shown in latitude × pressure indicate that the seasonal signals can be highly variable in space and from one season to another and are often not significant at the 95% confidence level.
6. Even with the very long (165 year) time series, it is not possible for MLR analysis to cleanly separate the attributions to CO_2 and to EESC. Both forcings lead to cooling in the stratosphere and are driven by similar rapid growth of anthropogenic emissions in the second half of the 20th century. This is an important new result that should be a concern for other model and observational analyses as well.

Data Availability Statement

The computing and data storage resources including Cheyenne super computer (http://10.5065/D6RX99HX) were provided by the Computational and Information Systems Laboratory (CISL) at NCAR. The archived model data used in this study can be obtained from online (https://esgf-node.llnl.gov/projects/cmip6/). WACCM6 code is available as part of the CESM2 release via github, and the instructions are available online (at: http://www.cesm.ucar.edu/models/cesm2/release_download.html). Simulations shown in this work for WACCM6 historical and coupled experiments are available as part of the Coupled Model Intercomparison Project Round 6 (CMIP6) on the Earth System Grid.

Acknowledgments

The authors acknowledge the pioneering work by the progenitors of whole atmosphere modeling and many members of WACCM. Many thanks to Liying Qian of HAO and Charles G. Bardeen of ACOM for their helpful comments and suggestions on the original manuscript. This research is supported by the NASA Living With a Star (LWS) Jack Eddy Postdoctoral Fellowship Program, administered by UCAR's Cooperative Programs for the Advancement of Earth System Science (CPAESS) under award #NNX16AK22G. One of the authors (K. Ramesh) is thankful to UCAR and NASA for the support through above fellowship. The National Center for Atmospheric Research (NCAR) is sponsored by the National Science Foundation (NSF). The authors are thankful to the Editor and the two anonymous reviewers for their critical comments and suggestions, which greatly helped to improvise the manuscript.

References

Akmaev, R. A. (2012). On estimation and attribution of long-term temperature trends in the thermosphere. *Journal of Geophysical Research*, *117*, A09321. https://doi.org/10.1029/2012JA018058

Akmaev, R. A., & Fomichev, V. I. (1998). Cooling of the mesosphere and lower thermosphere due to doubling of CO_2. *Annales de Geophysique*, *16*, 1501–1512.

Akmaev, R. A., Fomichev, V. I., & Zhu, X. (2006). Impact of middle-atmospheric composition changes on greenhouse cooling in the upper atmosphere. *Journal of Atmospheric and Solar - Terrestrial Physics*, *68*(17), 1879–1889. https://doi.org/10.1016/j.jastp.2006.03.008

Andersson, S., Martinsson, B., Vernier, J., Friberg, J., Brenninkmeijer, C. A. M., Hermann, M., et al. (2015). Significant radiative impact of volcanic aerosol in the lowermost stratosphere. *Nature Communications*, *6*(1), 7692. https://doi.org/10.1038/ncomms8692

Andrews, D. G., Holton, J. R., & Leovy, C. B. (1987). *Middle atmosphere dynamics*. San Diego, California: Academic Press.

Beig, G., Keckhut, P., Lowe, R. P., Roble, R. G., Mlynczak, M. G., Scheer, J., et al. (2003). Review of mesospheric temperature trends. *Reviews of Geophysics*, *41*(4), 1015. https://doi.org/10.1029/2002RG000121

Chiodo, G., Marsh, D. R., Garcia-Herrera, R., Calvo, N., & García, J. A. (2014). On the detection of the solar signal in the tropical stratosphere. *Atmospheric Chemistry and Physics*, *14*(11), 5251–5269. https://doi.org/10.5194/acp-14-5251-2014

Danabasoglu, G., Lamarque, J.-F., Bacmeister, J., Bailey, D. A., DuVivier, A. K., Edwards, J., et al. (2020). The Community Earth System Model Version 2 (CESM2). *Journal of Advances in Modeling Earth Systems*, *12*, e2019MS001916. https://doi.org/10.1029/2019MS001916

Diallo, M., Ploeger, F., Konopka, P., Birner, T., Müller, R., Riese, M., & Jegou, F. (2017). Significant contributions of volcanic aerosols to decadal changes in the stratospheric circulation. *Geophysical Research Letters*, *44*, 10,780–10,791. https://doi.org/10.1002/2017GL074662

Free, M., & Seidel, D. J. (2009). Observed El Niño-Southern Oscillation temperature signal in the stratosphere. *Journal of Geophysical Research*, *114*, D23108. https://doi.org/10.1029/2009JD012420

Garcia, R. R., López-Puertas, M., Funke, B., Kinnison, D. E., Marsh, D. R., & Qian, L. (2016). On the secular trend of CO and CO_2 in the lower thermosphere. *Journal of Geophysical Research: Atmospheres*, *121*, 3634–3644. https://doi.org/10.1002/2015JD024553

Garcia, R. R., Marsh, D. R., Kinnison, D. E., Boville, B. A., & Sassi, F. (2007). Simulations of secular trends in the middle atmosphere, 1950–2003. *Journal of Geophysical Research*, *112*, D09301. https://doi.org/10.1029/2006JD007485

Garcia, R. R., Smith, A. K., Kinnison, D. E., de la Cámara, Á., & Murphy, D. J. (2017). Modification of the gravity wave parameterization in the Whole Atmosphere Community Climate Model: Motivation and results. *Journal of the Atmospheric Sciences*, *74*(1), 275–291. https://doi.org/10.1175/JAS-D-16-0104.1

Garcia, R. R., Yue, J., & Russell, J. M. III (2019). Middle atmosphere temperature trends in the twentieth and twenty-first centuries simulated with the Whole Atmosphere Community Climate Model (WACCM). *Journal of Geophysical Research: Space Physics*, *124*, 7984–7993. https://doi.org/10.1029/2019JA026909

García-Herrera, R., Calvo, N., Garcia, R. R., & Giorgetta, M. A. (2006). Propagation of ENSO temperature signals into the middle atmosphere: A comparison of two general circulation models and ERA-40 reanalysis data. *Journal of Geophysical Research*, *111*, D06101. https://doi.org/10.1029/2005JD006061

Gettelman, A., Mills, M. J., Kinnison, D. E., Garcia, R. R., Smith, A. K., Marsh, D. R., et al. (2019). The Whole Atmosphere Community Climate Model Version 6 (WACCM6). *Journal of Geophysical Research: Atmospheres*, *124*, 12,380–12,403. https://doi.org/10.1029/2019JD030943

Gille, J. C., & Lyjak, L. V. (1986). Radiative heating and cooling rates in the middle atmosphere. *Journal of the Atmospheric Sciences*, *43*(20), 2215–2229. https://doi.org/10.1175/1520-0469(1986)043<2215:RHACRI>2.0.CO;2

Hansen, J., Sato, M., Ruedy, R., Lacis, A., Asamoah, K., Borenstein, S., et al. (1996). A Pinatubo climate modeling investigation. In G. Fiocco, D. Fua, G. Visconti (Eds.), *The Mount Pinatubo eruption: Effects on the atmosphere and climate*, *Nato ASI Series* (Vol. I 42, pp. 233–272). Heidelberg, Germany: Springer. https://doi.org/10.1007/978-3-642-61173-5_20

Krivolutsky, A. A., Cherepanova, L. A., & Dement'eva, A. V. (2015). Solar cycle influence on troposphere and middle atmosphere via ozone layer in the presence of planetary waves: Simulation with ARM. *Journal of Geophysical Research: Space Physics*, *120*, 8298–8306. https://doi.org/10.1002/2015JA021363

Kuhn, W. R., & London, J. (1969). Infrared radiative cooling in the middle atmosphere (30 km–110 km). *Journal of the Atmospheric Sciences*, *26*(2), 189–204. https://doi.org/10.1175/1520-0469(1969)026<0189:IRCITM>2.0.CO;2

Kutner, M. H., Nachtsheim, C. J., & Neter, J. (2004). *Applied linear regression models* (4th ed.). New York: McGraw-Hill Irwin.

Laštovička, J. (2017). A review of recent progress in trends in the upper atmosphere. *Journal of Atmospheric and Solar - Terrestrial Physics*, *163*, 2–13. https://doi.org/10.1016/j.Jastp.2017.03.009

Lee, S., Shelow, D. M., Thompson, A. M., & Miller, S. K. (2010). QBO and ENSO variability in temperature and ozone from SHADOZ, 1998–2005. *Journal of Geophysical Research*, *115*, D18105. https://doi.org/10.1029/2009JD013320

Li, T., Calvo, N., Yue, J., Dou, X., Russell, J. M. III, Mlynczak, M. G., et al. (2013). Influence of El Niño-Southern Oscillation in the mesosphere. *Geophysical Research Letters*, *40*, 3292–3296. https://doi.org/10.1002/grl.50598

Lübken, F.-J., Berger, U., & Baumgarten, G. (2013). Temperature trends in the midlatitude summer mesosphere. *Journal of Geophysical Research: Atmospheres*, *118*, 13,347–13,360. https://doi.org/10.1002/2013JD020576

Manzini, E., Giorgetta, M. A., Esch, M., Kornblueh, L., & Roeckner, E. (2006). The influence of sea surface temperatures on the northern winter stratosphere: Ensemble simulations with the MAECHAM5 model. *Journal of Climate*, *19*(16), 3863–3881. https://doi.org/10.1175/JCLI3826.1

Marsh, D. R., & Garcia, R. R. (2007). Attribution of decadal variability in lower-stratospheric tropical ozone. *Geophysical Research Letters*, *34*, L21807. https://doi.org/10.1029/2007GL030935

Marsh, D. R., Garcia, R. R., Kinnison, D. E., Boville, B. A., Sassi, F., Solomon, S. C., & Matthes, K. (2007). Modeling the whole atmosphere response to solar cycle changes in radiative and geomagnetic forcing. *Journal of Geophysical Research*, *112*, D23306. https://doi.org/10.1029/2006JD008306

Marsh, D. R., Mills, M. J., Kinnison, D. E., Lamarque, J., Calvo, N., & Polvani, L. M. (2013). Climate change from 1850 to 2005 simulated in CESM1(WACCM). *Journal of Climate*, *26*(19), 7372–7391. https://doi.org/10.1175/JCLI-D-12-00558.1

Matthes, K., Funke, B., Andersson, M. E., Barnard, L., Beer, J., Charbonneau, P., et al. (2017). Solar forcing for CMIP6 (v3.2). *Geoscientific Model Development*, *10*(6), 2247–2302. https://doi.org/10.5194/gmd-10-2247-2017

Mehta, S. K., Fujiwara, M., Tsuda, T., & Vernier, J. P. (2015). Effect of recent minor volcanic eruptions on temperatures in the upper troposphere and lower stratosphere. *Journal of Atmospheric and Solar - Terrestrial Physics*, *129*, 99–110. https://doi.org/10.1016/j.jastp.2015.04.009

Miles, J. (2014). Tolerance and variance inflation factor. In N. Balakrishnan, T. Colton, B. Everitt, W. Piegorsch, F. Ruggeri, J. L. Teugels (Eds.), *Wiley StatsRef: Statistics reference online*. Chichester, UK: John Wiley & Sons, Ltd. https://doi.org/10.1002/9781118445112.stat06593

Mills, M. J., Schmidt, A., Easter, R., Solomon, S., Kinnison, D. E., Ghan, S. J. III, et al. (2016). Global volcanic aerosol properties derived from emissions, 1990–2014, using CESM1(WACCM). *Journal of Geophysical Research: Atmospheres*, *121*, 2332–2348. https://doi.org/10.1002/2015JD024290

Mlynczak, M. G., Mertens, C. J., Garcia, R. R., & Portmann, R. W. (1999a). A detailed evaluation of the stratospheric heat budget: 1. Radiation transfer. *Journal of Geophysical Research*, *104*(D6), 6021–6038. https://doi.org/10.1029/1998JD200100

Mlynczak, M. G., Mertens, C. J., Garcia, R. R., & Portmann, R. W. (1999b). A detailed evaluation of the stratospheric heat budget: 2. Global radiation balance and diabatic circulations. *Journal of Geophysical Research*, *104*(D6), 6039–6066. https://doi.org/10.1029/1998JD200099

Mlynczak, M. G., & Solomon, S. (1993). A detailed evaluation of the heating efficiency in the middle atmosphere. *Journal of Geophysical Research*, *98*(D6), 10,517–10,541. https://doi.org/10.1029/93JD00315

Neely, R. R. III, & Schmidt, A. (2016). VolcanEESM: Global volcanic sulphur dioxide (SO2) emissions database from 1850 to present—Version 1.0. Centre for Environmental Data Analysis, 04 February 2016, doi:https://doi.org/10.5285/76ebdc0b-0eed-4f70-b89e-55e606bcd568. https://doi.org/10.5285/76ebdc0b-0eed-4f70-b89e-55e606bcd568

Newman, P. A., Daniel, J. S., Waugh, D. W., & Nash, E. R. (2007). A new formulation of equivalent effective stratospheric chlorine (EESC). *Atmospheric Chemistry and Physics*, *7*(17), 4537–4552. https://doi.org/10.5194/acp-7-4537-2007

O'brien, R. M. (2007). A caution regarding rules of thumb for variance inflation factors. *Quality and Quantity*, *41*(5), 673–690. https://doi.org/10.1007/s11135-006-9018-6

Oman, L., Robock, A., Stenchikov, G., Schmidt, G. A., & Ruedy, R. (2005). Climatic response to high-latitude volcanic eruptions. *Journal of Geophysical Research*, *110*, D13103. https://doi.org/10.1029/2004JD005487

Qian, L., Jacobi, C., & McInerney, J. (2019). Trends and solar irradiance effects in the mesosphere. *Journal of Geophysical Research: Space Physics*, *124*, 1343–1360. https://doi.org/10.1029/2018JA026367

Randel, W. J., Garcia, R. R., Calvo, N., & Marsh, D. (2009). ENSO influence on zonal mean temperature and ozone in the tropical lower stratosphere. *Geophysical Research Letters*, *36*, L15822. https://doi.org/10.1029/2009GL039343

Riese, M., Ploeger, F., Rap, A., Vogel, B., Konopka, P., Dameris, M., & Forster, P. (2012). Impact of uncertainties in atmospheric mixing on simulated UTLS composition and related radiative effects. *Journal of Geophysical Research*, *117*, D16305. https://doi.org/10.1029/2012JD017751

Roble, R. G., & Dickinson, R. E. (1989). How will changes in carbon dioxide and methane modify the mean structure of the mesosphere and thermosphere? *Geophysical Research Letters*, *16*(12), 1441–1444. https://doi.org/10.1029/GL016i012p01441

Robock, A. (2000). Volcanic eruptions and climate. *Reviews of Geophysics*, *38*(2), 191–219. https://doi.org/10.1029/1998RG000054

Rowland, F. S. (1991). Stratospheric ozone depletion. *Annual Review of Physical Chemistry*, *42*(1), 731–768. https://doi.org/10.1146/annurev.pc.42.100191.003503

Sassi, F., Kinnison, D., Boville, B. A., Garcia, R. R., & Roble, R. (2004). Effect of El Niño-Southern Oscillation on the dynamical, thermal, and chemical structure of the middle atmosphere. *Journal of Geophysical Research*, *109*, D17108. https://doi.org/10.1029/2003JD004434

Schmidt, H., Rast, S., Bunzel, F., Esch, M., Giorgetta, M., Kinne, S., et al. (2013). Response of the middle atmosphere to anthropogenic and natural forcings in the CMIP5 simulations with the Max Planck Institute Earth system model. *Journal of Advances in Modeling Earth Systems*, *5*, 98–116. https://doi.org/10.1002/jame.20014

Solomon, S., Ivy, D., Gupta, M., Bandoro, J., Santer, B., Fu, Q., et al. (2017). Mirrored changes in Antarctic ozone and stratospheric temperature in the late 20th versus early 21st centuries. *Journal of Geophysical Research: Atmospheres*, *122*, 8940–8950. https://doi.org/10.1002/2017JD026719

Solomon, S., Rosenlof, K. H., Portmann, R. W., Daniel, S. M., Davis, J. S., Sanford, T., & Plattner, G.-K. (2010). Contributions of stratospheric water vapor to decadal changes in the rate of global warming. *Science*, *327*(5970), 1219–1223. https://doi.org/10.1126/science.1182488

Sridharan, S., Tsuda, T., & Gurubaran, S. (2010). Long-term tendencies in the mesosphere/lower thermosphere mean winds and tides as observed by medium-frequency radar at Tirunelveli (8.7°N, 77.8°E). *Journal of Geophysical Research*, *115*, D08109. https://doi.org/10.1029/2008JD011609

Sridharan, S., Vishnu Prasanth, P., & Bhavani Kumar, Y. (2009). A report on long-term trends and variabilities in middle atmospheric temperature over Gadanki (13.5°N, 79.2°E). *Journal of Atmospheric and Solar - Terrestrial Physics*, *71*(13), 1463–1470. https://doi.org/10.1016/j.jastp.2008.09.017

Stolarski, R. S., Douglass, A. R., Newman, P. A., Pawson, S., & Schoeberl, M. R. (2010). Relative contribution of greenhouse gases and ozone-depleting substances to temperature trends in the stratosphere: A chemistry-climate model study. *Journal of Climate*, *23*(1), 28–42. https://doi.org/10.1175/2009JCLI2955.1

Tilmes, S., Hodzic, A., Emmons, L. K., Mills, M. J., Gettelman, A., Kinnison, D. E., et al. (2019). Climate forcing and trends of organic aerosols in the Community Earth System Model (CESM2). *Journal of Advances in Modeling Earth Systems*, *11*, 4323–4351. https://doi.org/10.1029/2019MS001827

Tilmes, S., Müller, R., & Salawitch, R. (2011). The sensitivity of polar ozone depletion to proposed geoengineering schemes. *Science*, *320*(5880), 1201–1204. https://doi.org/10.1126/science.1153966

Venkat Ratnam, M., Akhil Raj, S. T., & Qian, L. (2019). Long-term trends in the low-latitude middle atmosphere temperature and winds: Observations and WACCM-X model simulations. *Journal of Geophysical Research: Space Physics*, *124*, 7320–7331. https://doi.org/10.1029/2019JA026928

Venkat Ratnam, M., Kishore Kumar, G., Venkateswara Rao, N., Krishna Murthy, B. V., Laštovička, J., & Qian, L. (2013). Evidence of long-term change in zonal wind in the tropical lower mesosphere: Observations and model simulations. *Geophysical Research Letters*, *40*, 397–401. https://doi.org/10.1002/grl.50158

Wilks, D. S. (2006). *Statistical methods in the atmospheric sciences* (2nd ed.). San Diego, California: Academic Press.